Bull. Chem. Soc. Ethiop. **2025**, 39(4), 673-686.
DOI: https://dx.doi.org/10.4314/bcse.v39i4.6

ISSN 1011-3924
Printed in Ethiopia
Online ISSN 1726-801X

NEW (2Z)-1-(2,4-DINITROPHENYL)-2-[(2E)-3-(2-NITROPHENYL)PROP-2-EN-1-YLIDENE]HYDRAZINE AND ITS V(II) AND Ni(II) COMPLEXES: SYNTHESIS, CHARACTERIZATION AND *IN SILICO* SARS-CoV-2 INHIBITION STUDIES

K. O. Eberendu[1], C. I. Nwankwo[2], O. M. Mac-kalunta[3], J. I. Iheanyichukwu[3], I. E. Otuokere[3*], J. C. Nnaji[3] and I. O. Abaleke[4]

[1]Department of Chemistry, Spiritan University, Nneochi, Abia, Nigeria
[2]Department of Biochemistry, Michael Okpara University of Agriculture, Nigeria
[3]Department of Chemistry, Michael Okpara University of Agriculture, Nigeria
[4]Department of Healthcare Leadership, Faculty of Nursing Science, BPP University Waterloo, London, United Kingdom

(Received August 5, 2024; Revised December 31, 2024; Accepted January 3, 2025)

ABSTRACT. Hydrazones are an important family of compounds with an azomethine proton (-NHN=CH-), which have been reported to possess high biological activity such as antioxidants, anti-consultants, analgesics, antimicrobial, anti-protozoals, anti-parasitic, anti-platelets, cardio-protective, anti-diabetic, anti-HIV and anti-helminthic. This research was aimed at synthesizing a new aniline hydrazone and its V(II) and Ni(II) complexes, and *in silico* SARS-CoV-2 inhibition studies. The (2*Z*)-1-(2,4-dinitrophenyl)-2-[(2*E*)-3-(2-nitrophenyl)prop-2-en-1-ylidene]hydrazine (DNEAA) was synthesized by the reaction of 2,4-dinitrophenylhydrazine and 3-(2-nitrophenyl)prop-2-enal. DNEAA and its V(II) and Ni(II) complexes were synthesized and characterized by UV-visible, FTIR, and NMR spectroscopy. Molecular docking was performed using Auto Dock Vina software. Spectroscopic analysis suggested that DNEAA coordinated with the metal ions through azomethine nitrogen, NH, two NO_2 and two Cl^-. An octahedral geometry was proposed for the metal complexes. The ability of DNEAA to chelate V(II) and Ni(II) is hereby assured. Molecular docking results gave binding energies >9.5 kcal/mol. Following these findings, it is recommended that biological studies and preclinical and clinical trials against SARS-CoV-2 protease be carried out.

KEY WORDS: 2,4-Dinitro-N-[(E)-[(E)-3-(2-nitropenyl)prop-2-enyildene]amino]aniline, Vanadium(II), Nickel(II), SARS-CoV-2, Molecular docking

INTRODUCTION

Among the numerous organic compounds with versatile applications, hydrazones have provided a formidable center for research [1–12]. The C=N double bond in hydrazones is an important functionality in drug design [13]. Because of their capacity to coordinate and their biological activities, hydrazone compounds involving O, N, and S donor ligands have attracted particular attention in terms of their chemistry [14]. Utilizing hydrazones offers a chance to improve drug design by releasing the medication at specified sites, including thrombosis or tumor tissue. In particular, employing heat and chemical catalysts to efficiently synthesize these hydrazones is a topic of much investigation. Two of the numerous distinctive characteristics of hydrazones that make them useful in drug development are their reactions to pH environments and their ease of synthesis for groups. Furthermore, because of their adaptability, they can be used in a variety of applications, such as chelating agents, anti-inflammatory, and anticancer [14, 15]. Many research investigations have demonstrated that the lone pair of electrons on the trigonally orientated nitrogen atom of the C=N group of hydrazones is what is responsible for their chemical and biological activity [16]. Other reported applications of hydrazones and their derivatives can include their biological uses as anti-oxidants, anti-consultants, analgesics, anti-microbial, anti-

*Corresponding authors. E-mail: ifeanyiotuokere@gmail.com

protozoals, anti-parasitic, anti-platelets, cardio-protective, anti-diabetic, anti-HIV, anti-helminthic, anti-tubercular, and so on [17]. These highlighted bioactivities of hydrazones and associated metal complexes have sparked interest in developing a new hydrazone that will be tested for bioactivity against SARS-CoV-2 [18].

Major concerns for all societal sectors worldwide are the highly contagious characteristics of SARS-CoV-2 and its quick transfer from person to person through droplets or direct communication [19]. A novel coronavirus was discovered in late 2019 [20]. The emergence of this disease resulted in the COVID-19 pandemic, which caused widespread concern due to its high pollution levels, ability to spread rapidly, and high mortality rate. The causative agent of COVID-19 is a beta coronavirus, which has a nucleotide similarity of 89.1% with the SARS-CoV [21]. Efforts were implemented to counteract the transmission of COVID-19 [22]. Research has shown evidence that the antimalarial and autoimmune disease medications chloroquine (CQ) and hydroxychloroquine (HCQ) can prevent viral infection by raising the pH levels in endosomes. As a result, the FDA has granted approval for these drugs [23–26]. Remdesivir (RDV) and its active metabolites have been shown to effectively limit the growth of SARS-CoV-2 in clinical settings when used as combination therapy [27–29]. Arbidol (ARB, umifenovir), a virus-host cell fusion inhibitor, is a broad-spectrum antiviral medication that is now being tested in a clinical trial for the treatment of COVID-19 [30, 31].

Computational chemists have been highly focused on the virtual screening of compounds that can effectively inhibit the harmful effects of SARS-CoV-2 due to its efficiency, cost-effectiveness, improved predictive accuracy, personalized and targeted applications, and potential to revolutionize drug discovery and material design. In this study, we have used in silico techniques to analyze a new aniline hydrazone DNEAA and its V(II) and Ni(II) complexes. Our aim is to determine if DNEAA and its V(II) and Ni(II) complexes could be a potential pharmaceutical option for blocking the harmful activities of SARS-CoV-2's NSP1 protein. The objective of conducting this computational analysis using the new ligand is to identify crucial amino acid residues in the substrate-binding pocket. This information can be used for structure-based drug design, enabling the use of the molecule as a blueprint for synthesizing new inhibitors and repurposing other types of molecules.

EXPERIMENTAL

Synthesis of DNEAA

This experiment utilized only analytical-grade chemicals and reagents, imported from Sigma Aldrich, and were used without further treatment. The chemicals include 2,4-dinitrophenylhydrazine, (2,4-DNP), and 3-(2-nitrophenyl)prop-2-enal. DNEAA was prepared in the manner described in literature [13, 32]. To the clear solution obtained by filtering a warmed mixture of 1.99 g (0.01 mol.) of 2,4-DNP, 10 mL of concentrated H_2SO_4, 15 mL of water, and 25 mL of methanol, 1.77 g (0.01 mol.) of the carbonyl compound 3-(2-nitrophenyl)prop-2-enal was added and heated just to boiling (Scheme 1). The precipitates formed were allowed to cool to room temperature before they were recrystallized from methanol and dried.

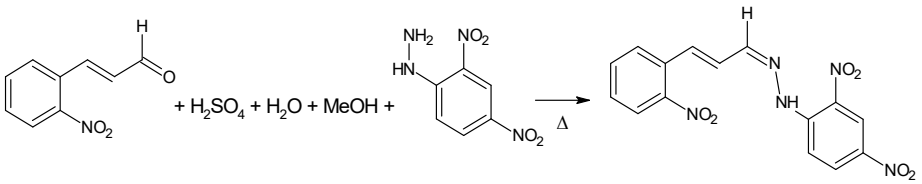

Scheme 1. Synthesis of DNEAA.

Synthesis of the DNEAA metal complexes

The DNEAA metal complexes were prepared by methods outlined by Prushan [33]. Exactly 1.22 g (0.01 mol) of VCl_2 was dissolved in 5 mL of methanol; the mixtures were stirred for 5 min. A solution of the DNEAA ligand obtained by dissolving 3.57 g of the newly synthesized compound separately in a hot solution of methanol solvent was added to the solution of the metal salts and stirred. The obtained product was cooled, re-crystalized with methanol solvent, and dried at room temperature. The same procedure was repeated with 1.30 g (0.01) $NiCl_2$. Equations of reactions are shown in 1 and 2.

$$VCl_2 + DNEAA \xrightarrow{MeOH} [V(DNEAA)Cl_2] \quad (1)$$

$$NICl_2 + DNEAA \xrightarrow{MeOH} [Ni(DNEAA)Cl_2] \quad (2)$$

Physical measurements

Melting points were recorded using Mettler Toledo's MT 211 melting point apparatus from Mettler Company. Elemental analysis for C, H and N were determined using an EA 2400 Series II analyzer. A solubility check was carried out in common solvents (DMF, DMSO, water, ethanol, and methanol) at 25 °C using 1 g.

Characterization

The UV/Visible spectra of DNEAA and the complexes were obtained using a UV-1800 series. DMSO was used as solvent. The "KBr Pellet Technique" was used to record the infrared spectra using Perkin-Elmer (Model C91158) IR spectrophotometer. The NMR spectrum was recorded using a JEOL GSX-400 spectrometer.

Molecular docking

Molecular docking binding affinity assessments were performed using Auto Dock Vina, which was constructed in the PyRx software. The structure of the DNEAA and its V(II) and Ni(II) complexes were drawn using ChemDraw version 18.0 from PerkinElmer Informatics, Inc. The 7K3N's coordinates were made available from the protein data bank. The default settings of the ArgusLab 4.0.1 software were utilized to prepare the protein and ligand structures. All docked complexes, bond lengths, types of interactions, and three-dimensional images were all visualized using Protein-Plus and the Protein-Ligand Interaction Profiler Servers. The quality of the interactions between the biomolecules was assessed using binding affinity analysis.

RESULTS AND DISCUSSION

Table 1 presents the physical properties of DNEAA, and its metal complexes. The ligand and its metal complexes are, colored, crystalline, and, air-stable at room temperature. They are soluble in both dimethylformamide and dimethyl sulfoxide, but insoluble in water, ethanol, and methanol (Table 2). The percentage yield of the synthesized hydrazones is 91%, while those of the metal complexes are 89 and 85%. This showed that the methods employed for the syntheses were efficient. Melting points determined are shown in Tables 4.1 and 4.2. The molar conductance values (10^{-4} M) (Table 2), lie in the range of non-electrolytes 50 and 48 $Ohm^{-1}cm^2mol^{-1}$) for the V, and Ni complexes, respectively, which confirmed coordination of the anions to the metal ions [34].

Table 1. Physical properties of DNEAA and its metal complexes.

Compounds	Color	M.P. (ºC)	Yield (%)	Found (calc.) (%)		
				C	H	N
DNEAA	Yellowish-red	115	91	50.40 (50.43)	3.50 (3.10)	19.90 (19.60)
[V(DNEAA)Cl_2]	Purple	135	89	38.00 (37.60)	2.42 (2.31)	14.64 (14.62)
[Ni(DNEAA)Cl_2]	Green	152	85	37.40 (37.00)	2.29 (2.28)	14.449 (14.38)

Table 2. Molar conductivity and solubilities of DNEAA and its metal complexes.

Compounds		Solubility ratings (25 ºC)				
	Molar conductivity ($Ohm^{-1}cm^2mol^{-1}$)	DMF	DMSO	Water	Ethanol	Methanol
DNEAA	-	3	3	2	2	2
[V(DNEAA)Cl_2]	50	3	3	1	1	1
[Ni(DNEAA)Cl_2]	48	3	3	1	1	1

Note: 3 = Very soluble, 2 sparingly soluble and 1= insoluble.

Electronic spectra of the DNEAA and its metal complexes.

Figures 1a-c shows the UV-Visible spectra of DNEAA and its metal complexes recorded in ethanol solutions between 200 and 800 nm at 25 °C. In the spectrum of the free ligand (DNEAA), the band at 379 nm was attributed to $\pi \rightarrow \pi^*$ transition of the azomethine moieties [35]. This transition is known as intra-ligand charge transfer (ILCT), and was shifted to longer or shorter wavelengths in the spectra of the metal complexes. Consequently, the bands at 255 and 330 nm were attributed to $\pi \rightarrow \pi^*$ transitions for [V(DNEAA)Cl_2], and [Ni(DNEAA)Cl_2] complexes, respectively. The observed shift in wavelengths is a consequence of the coordination of the DNEAA ligand to the various metal centers [35].

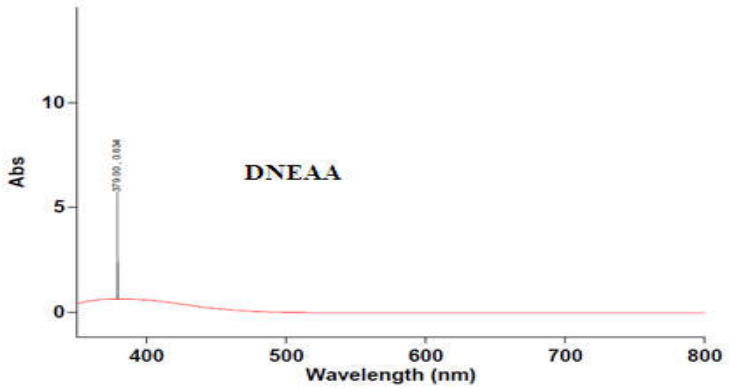

Figure 1a. Electronic spectrum of DNEAA.

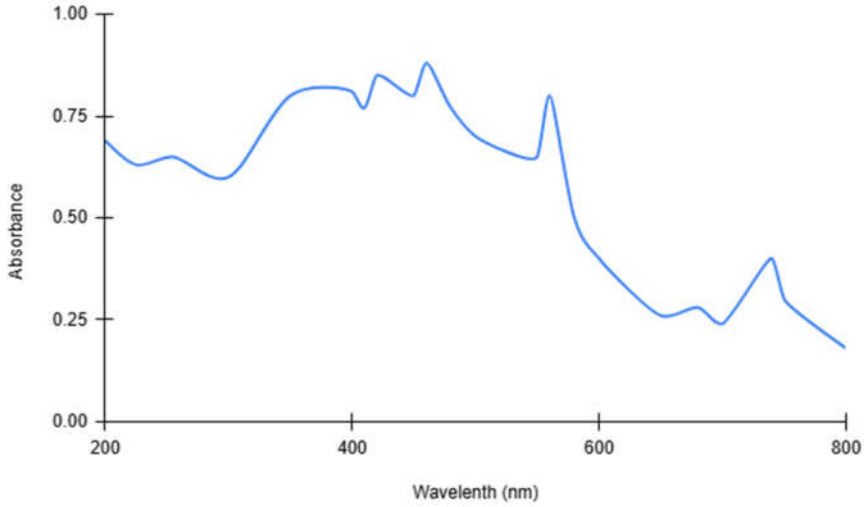

Figure 1b. Electronic spectrum of [V(DNEAA)Cl_2].

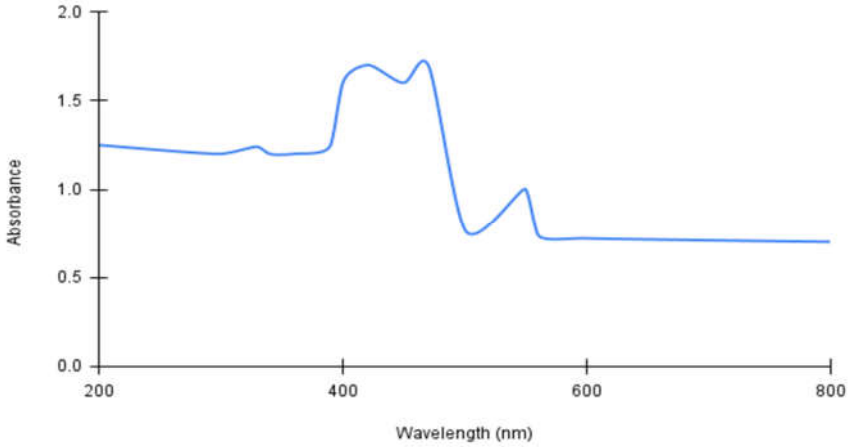

Figure 1c. Electronic spectrum of [Ni(DNEAA)Cl_2].

The ligand to metal charge transition (LMCT) was observed in the spectrum of the [V(DNEAA)Cl_2] complex at 420, 460, and 560 nm. These indicated the formation of an M-L coordination bond [36]. The bands at 680 and 740 nm were assigned to $T_1g(F) \rightarrow T_2g(F)$ and $T_1g(F) \rightarrow T_2g$ (P), transitions, respectively, suggesting the octahedral geometry around the [V(DNEAA)Cl_2] [32]. In the spectrum of the [Ni(DNEAA)Cl_2] complex, the bands at 420 and 470 nm was assigned to LMCT, while the band at 550 were attributed to $T_1g(F) \rightarrow T_2g(F)$ and $T_1g(F)$ [37].

Infrared spectra of the DNEAA and its metal complexes

The FTIR spectra of the ligand and metal complexes are presented in Figures 2a–c. Comparison of the FTIR spectra of DNEAA and metal complexes were made. The broad bands observed in the wavenumber range of 3324.8 cm^{-1} was due to the stretching frequency of the hydrogen bonding of the –NH group in the ligand. This vibration frequency was lowered to 3283.8 and 3235.3 cm^{-1} in the spectra of $[V(DNEAA)Cl_2]$ and $[Ni(DNEAA)Cl_2]$ complexes. This suggested that complexation occurred through NH group. The coordination of the ligand through the amide group(s) is mostly expected as seen in some amide complexes. [35, 35]. Increase in electron density, increased the N-H bond length and consequently slowed down the vibration frequency. The bond length is inversely related to the bond strength. In case of an increase in electron density around nitrogen, it repelled the electron cloud of hydrogen atoms. Because of this repulsion, the bond gets elongated. Moreover, the lone pair of nitrogen atom may cause greater repulsion on the bonding electrons and therefore the bond lengthening. The aromatic bending of –CH group of the ligand and metal complexes were observed at a frequency range of 920.7–872.2 cm^{-1}. Strong peaks observed at a frequency range of 1636.3 cm^{-1} corresponded to the vibrations of the -C=N group of the ligand. Lowering of the frequency to 1625.1 and 1617.7 cm^{-1} in the complexes showed that the azomethine group actively took part in co-ordination [37]. This is because it contains a carbon-nitrogen double bond, >C=N-, in which nitrogen is more electronegative than carbon. The azomethine group exerts a lone pair of electrons on nitrogen, hence this group is an excellent electron donor for coordination with metal ions. In one study, azomethine ligands showed a characteristic C=N band at ca. 1620 cm^{-1}, which was shifted by 10-15 cm^{-1} to lower wavenumbers upon coordination to the metal ions, reflecting the donation of the azomethine nitrogen in chelation [38]. These are also in agreement with the recorded shifts to 1625.1 cm^{-1} and 1617.7 cm^{-1}. To show a same mechanism from different metal complexes, studies on transition metal complexes showed that coordination with metals like cobalt, nickel, and copper also caused shifts of the C=N band to lower frequencies, normally in the range of 1605-1615 cm^{-1} [39]. The lower frequency bands observed at 738.0 and 685.8 cm^{-1} which were absent in the spectrum of the ligand and observed in the metal complexes are attributed to the vibrations due to M-N, which are strong indications of coordination [40]. The bands at the lower regions of the spectra 624.76 and 614.71 cm^{-1} are the M-Cl vibrational frequencies respectively, which showed that Cl^- are involved in coordination [41].

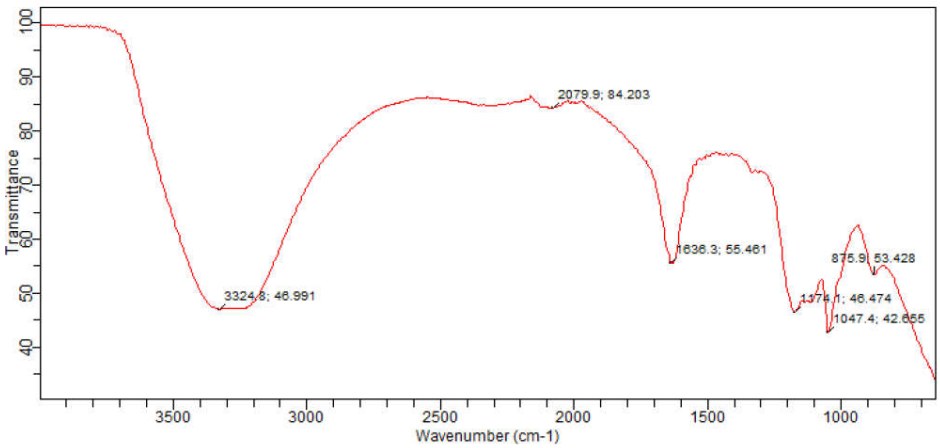

Figure 2a. FTIR Spectrum of DNEAA.

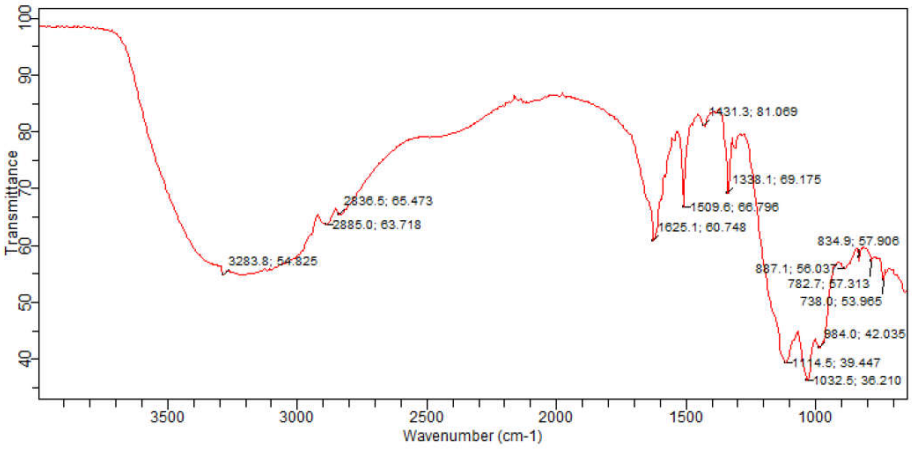

Figure 2b. FTIR Spectrum of [(V-DNEAA)Cl_2].

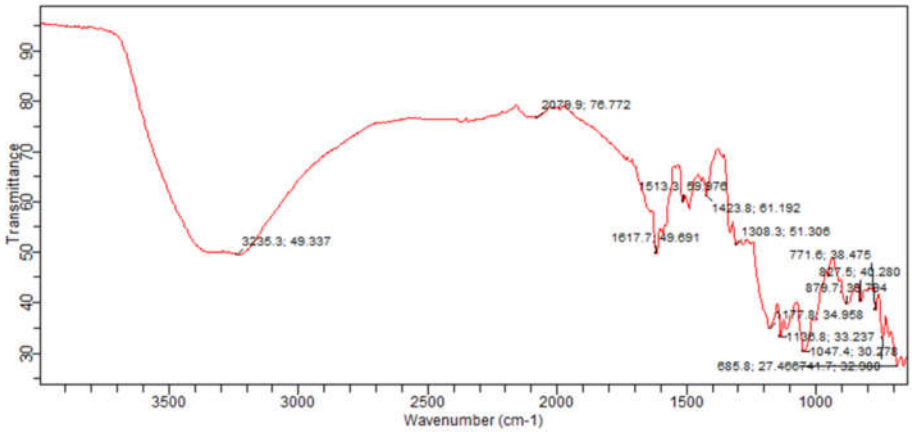

Figure 2c. FTIR Spectrum of [Ni(DNEAA)Cl_2].

NMR of the DNEAA and its metal complexes

The ^{1}H NMR spectra of the protons of interest resonated at their different distinct regions of the chemical shift as shown in Figures 3a-c. The signal of the azomethine proton (–HC=N–) was observed at 9.1 ppm in the spectrum of DNEAA. In the spectra of the complexes, the signal was shifted downfield to 9.9 ppm. This suggested that the azomethine proton was involved in complexation. Similar chemical shifts were observed by Asogwa and Otuokere [42]. The signals for the aromatic protons are seen as multiplet peaks in the range of 7.5-8.0 ppm in the ligand and complexes. Similarly, there is always a deshielding effect in the plane of the C=C bond due to π-electron (anisotropy) and steric effects [41]. These effects are responsible for the observed signals at δ = 6.0-7.0 ppm, which represent the protons attached to the olefinic carbon (H–C=C-H). For the N-H peak, it was clear that the effects of an electronegative nitrogen atom

caused its deshielding and shifting of its peak downfield to 11.9 ppm in the ligand. This peak was shifted to 12.7 ppm in the spectrum of the complexes. The electron density around the NH proton reduced as the NH group formed complexes with the V(II) and Ni(II) ion. This deshielding effect led the NH proton to resonate at a lower field, which in turn produced a downfield shift (higher ppm value) in the NMR spectrum. This shift suggested that N-H proton was involved in complexation. Further, the two multiplets that occurred at the range of 7.5-8.0 ppm are evident that there are two aromatic rings in the DNEAA and complexes whose protons resonated within the range of chemical shift reported.

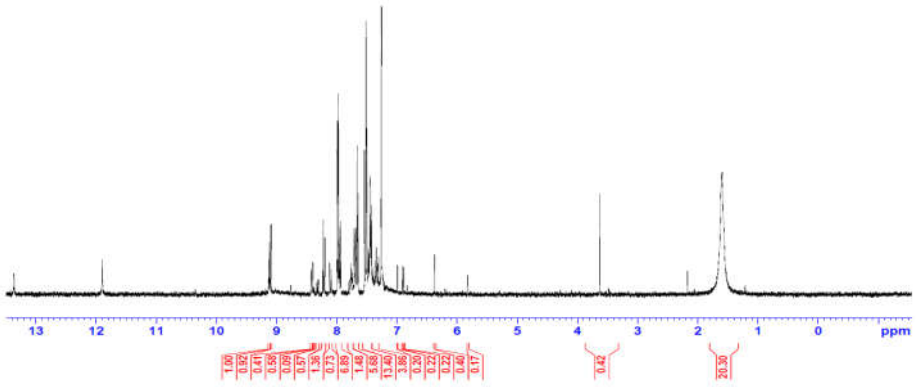

Figure 3a. ^{1}H NMR spectrum of DNEAA.

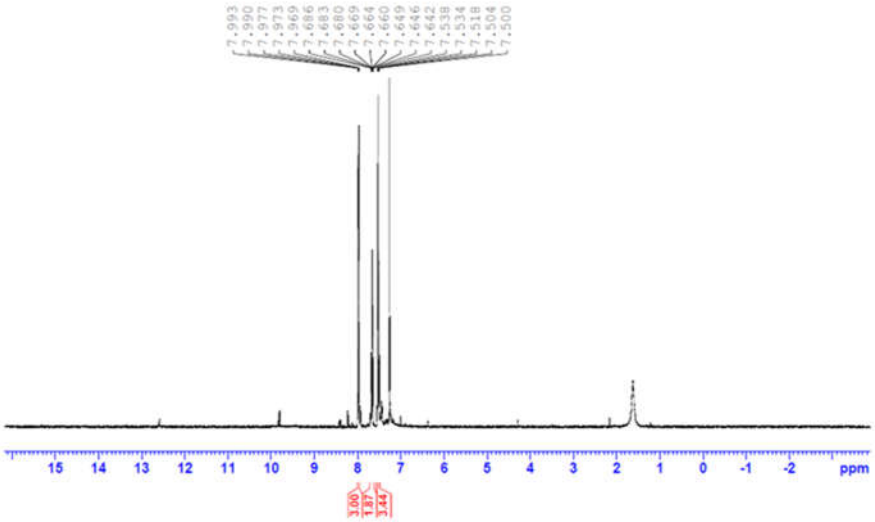

Figure 3b. ^{1}H NMR spectrum of [V(DNEAA)Cl_2].

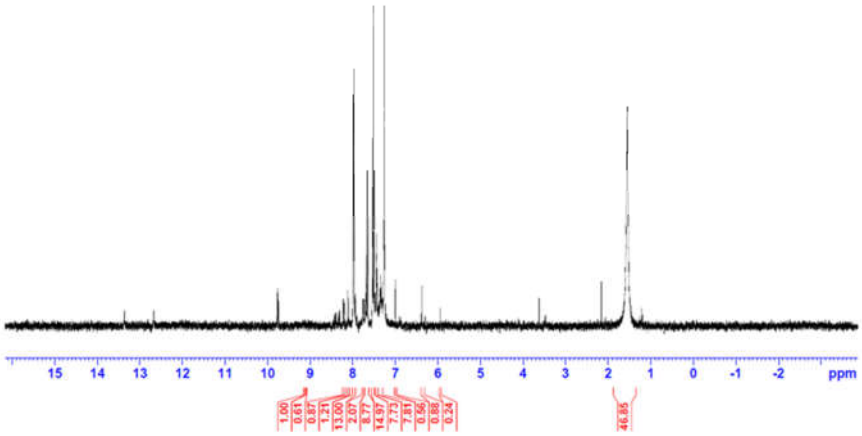

Figure 3c. ^{1}H NMR spectrum of [Ni(DNEAA)Cl_2].

The C-13 spectra are presented in Figures 4a-c.

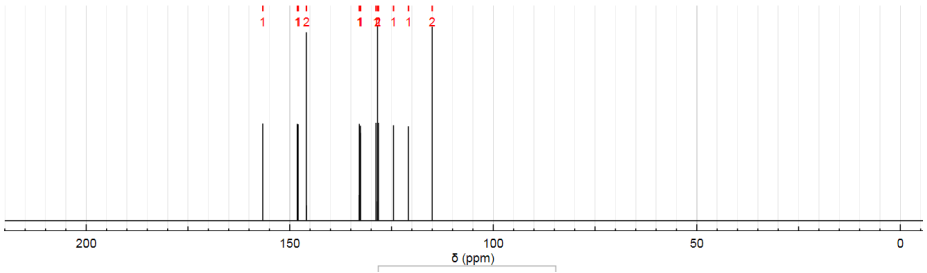

Figure 4a. ^{13}C-NMR spectrum of DNEAA.

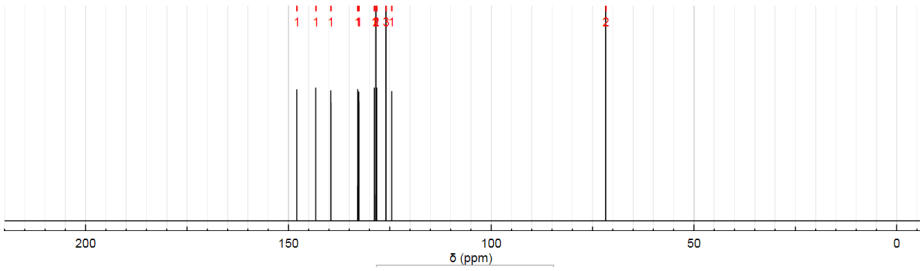

Figure 4b. ^{13}C-NMR spectrum of [V(DNEAA)Cl_2].

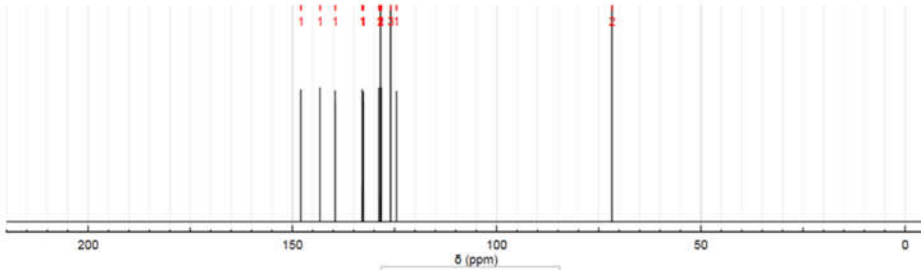

Figure 4c. ^{13}C-NMR spectrum of [Ni(DNEAA)Cl_2]

The signal due to the carbon atom attached to the azomethine group in the DNEAA was observed at δ 156.6 ppm. However, in the spectra of the corresponding metal complexes, the chemical shift resonated to δ 143.3 ppm. This indicated the coordination of the nitrogen atom of the azomethine group with the central metal ion. Coordination of the ligand to the various metals was shown by a new peak at δ 125.9 ppm, which was absent in the spectrum of the ligand. The signal shift due to aromatic ring carbons with various substitutions was observed in the range of 124.5-147.9 ppm for the ligand and complexes.

Based on spectroscopic information, the structures in Figures 5a and b have been proposed for the V(II) and Ni(II) complexes of DNEAA.

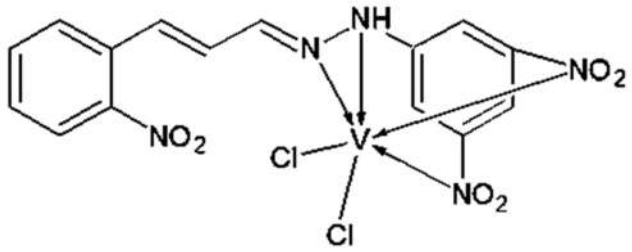

Figure 5a. Proposed structure of [V(DNEAA)Cl_2].

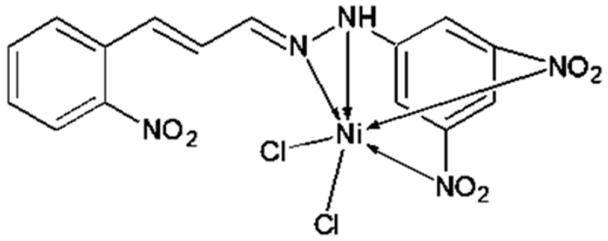

Figure 5b. Structure of the [Ni(DNEAA)Cl_2].

The binding affinities and interactions of DNEAA and its metal complexes with SARS-CoV-2 are presented in Table 3. The 3D interactions are presented in Figure 6.

Table 3. Binding affinities and interactions of DNEAA and its complexes with SARS-CoV-2.

Compound	Binding affinity kcal/mol	Hydrophobic interactions	Hydrogen bonding	Salt bridges
DNEAA	-10.3	LEU 12A, GLN 13A, VAL 14A, GLU 46A	VAL 11A, GLN 13A, VAL 14A, GLU 46A	-
[V(DNEAA)Cl_2]	-9.5	VAL 11A, GLN 13A, VAL 14A, GLU 46A	VAL 14A, GLU 46A	-
[Ni(DNEAA)Cl_2]	-9.5	GLN 13A, VAL 14A	VAL 14A, GLU 46A	GLU 46A
Azithromycin	-6.4		SER 63C, SER 64C, GLY 64C, GLY 66C, GLN 67C, HIS 69C	-

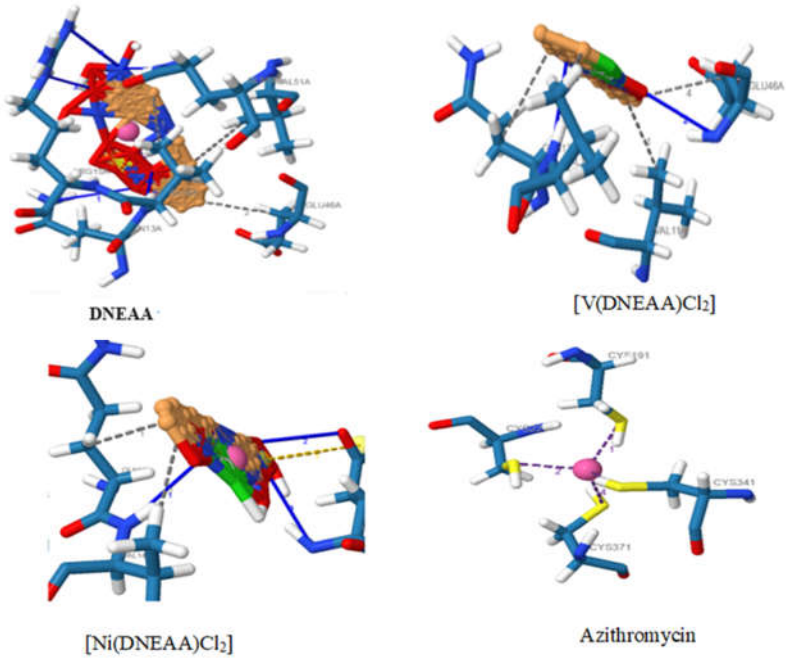

Figure 6. The 3D interactions of DNEAA and its complexes with SARS-CoV-2 protein.

The binding affinities (Table 3) indicated that DNEAA and its complexes have the ability to inhibit the SARS-CoV-2 protease. Their binding affinities were better than the FDA approved drug, azithromycin. The DNEAA conjugated systems and functional groups formed hydrogen bonding with the target. For the [V(DNEAA)Cl_2] and [Ni(DNEAA)Cl_2], the additional coordination sites provided by the central metal atom stabilize specific binding conformations and increase affinity. The 3D interactions of the DNEAA and its metal complexes

with SARS-CoV-2 have been shown in Figure 6. Different fragment hits were observed for the ligand-protein interactions. A summary of the amino acids interacting with the ligand and complexes at the allosteric binding sites has been presented in Table 6. For the DNEAA, hydrophobic interactions were observed at LEU 12A, GLN 13A, VAL 14A, and GLU 46A with distances of 3.48, 3.67, 3.72, 3.94, and 3.73 Å, respectively. Also, hits were observed at VAL 11A, GLN 13A, VAL 14A, and GLU 46A with bond distances 3.34, 3.23, 2.66, 3.17, and 3.56 Å, respectively, for hydrogen bond interactions. Similar interactions consisting of a substituted phenyl ring connected to the conjugated azomethine group of the hydrazone ligand have also been reported [43].

Hydrophobic interactions for the [V(DNEAA)Cl_2] complex were observed at fragment hits, VAL 11A and GLN 13A, VAL 14A and GLU 46A at distances of 3.53 and 3.71 Å, respectively, while hydrogen bonding interactions were observed at VAL 14A and GLU 46A at distances of 4.01 and 3.13 Å respectively. For the [Ni(DNEAA)Cl_2] interactions with 7K3N, fragment hits were observed for hydrophobic interaction at GLN 13A and VAL 14A at distances of 3.65 and 3.76 Å, respectively. Hydrogen bonding interactions were observed at VAL 14A, and GLU 46A at distances of 3.36, 3.38, and 3.61 Å, respectively. Salt bridge was observed at GLU 46A at a distance of 4.52 Å, respectively. According to the analysis of the 3D interactions, hydrogen bonding, which is a characteristic marker of strong interactions between proteins and ligands and frequently results in increased binding affinity, was found to be less prevalent than hydrophobic interactions. Usually, an increase in the amount of H-bonds in such interactions increases the inhibitory potential towards the target [25].

CONCLUSION

Synthesis and characterization of DNEAA and its V(II) and Ni(II) complexes were carried out. The metal complexes were characterized based on the observed FTIR spectra, electronic spectra, melting point, solubility, proton, and carbon-13 nuclear magnetic resonance. An octahedral structure was proposed for the complexes. The ability of DNEAA to chelate V(II) and Ni(II) is hereby assured. Molecular docking results showed that DNEAA and its complexes have the tendency to inhibit SARS-CoV-2 protease. Following these findings, more research on biological interactions, as well as pre- and clinical trials, is advised in relation to the SARS-CoV-2 protease.

REFERENCES

1. Mondal, S.K.; Chenglin, W.; Nwadire, F.C.; Rownaghi, A.; Kumar, A.; Adewuyi, Y.; Okoronkwo, M.U. Examining the effect of a chitosan biopolymer on alkali-activated inorganic material for aqueous Pb(II) and Zn(II) sorption. *Lang*. **2022**, 38, 903-913.
2. Otuokere, I.E.; Ohwimu, J.G.; Amadi, K.C.; Alisa, C.O.; Nwadire, F.C.; Igwe, O.U.; Okoyeagu, A. A. Ngwu. C.M. Synthesis, characterization and molecular docking studies of Mn(II) complex of sulfathiazole. *J. Nig. Soc. Phys. Sci.* **2019**, 1, 95-102.
3. Otuokere, I.E.; Okorie, D.O.; Asogwa, B.C.; Amadi, O.K.; Ubani, L.O.C.; Nwadire, F.C. Spectroscopic and coordination behavior of ascorbic acid towards copper(II) Ion. *Res. Anal. Bio. Chem*. **2017**, 1, 1-7.
4. Edozie, I.O.; Godday, O.J.; Chijioke, A.K.; Uchenna, I.O.; Chigozie, N.F. Synthesis, characterization and molecular docking studies of Co(II) metal complex of sulfathiazole. *Bull. Chem. Soc. Ethiop*. **2020**, 34, 83-92.
5. Otuokere, I.E.; Okpara, L.O.; Amadi, K.C.; Alisa, C.O.; Okoyeagu, A.; Nwadire, F.C. 4-N-(7-Chloroquinolin-4-yl)-1-N, 1-N-diethyl petane-1,4-diamine Ti complex: Synthesis and characterization. *BP Inter*. **2021**, 142-149.
6. Godwin, J.; Nwadire, F.C.; Uzoukwu, B.A. Extraction of Ni(II) ions into $CHCl_3$ solution of N,N'-ethylenebis (4-butanoyl-2,4-dihydro-5-methyl-2-phenyl-3h-pyrazol-3-one imine) Schiff base. *Eur. Chem. Bull*. **2012**, 1, 269-273.

7. Otuokere, I.E.; Nwaiwu, K.C.; Nwadire, F.C.; Akoh, O.U. Synthesis and characterization of Cr(III)-ascorbic acid complex. *J. Appl. Sci. Environ. Mgt*. **2022**, 26, 75-80.
8. Otuokere, I.E.; Okpara, L.O.; Amadi, K.C.; Ikpo, N.; Okafor, G.U.; Nwadire, F.C. Synthesis, characterization and complexation of Cr(III) ion using chloroquine diphosphate. *Drug. J. Chem. Soc. Nig.* **2019**, 49, 107-114.
9. Amadi, O.K.; Otuokere, I.E.; Bartholomew, C.F. Synthesis, characterization, in vivo antimalarial studies and geometry optimization of lumefantrine/artemether mixed ligand complexes. *Res. J. Pharm. Dos. Forms Technol.* **2015**, 7, 59-68.
10. Asogwa, B.C.; Mac-kalunta, O.M.; Iheanyichukwu, J.I.; Otuokere, I.E.; Nnochirionye, K. Sonochemical synthesis, characterization, and ADMET studies of Fe(II) and Cu(II) nano-sized complexes of trimethoprim. *J. Nig. Soc. Phys. Sci.* **2024**, 6, 1-11.
11. Otuokere, I.E.; Asogwa, B.C.; Nwadire, F.C.; Akoh, O.U.; Nwankwo, C.I.; Emole, P.O.; Elemike, E.E. Biological potentials of some Schiff bases and their chelates: A short review. *IntechOpen* **2024**, 1-17. http://dx.doi.org/10.5772/intechopen.114862.
12. Nwadire, F.C.; Ubani, C.O.; Otuokere, I. E.; Igwe, O.U.; Chilaka, J.N.; Chukwuemeka, H.O. Effects of acids, anions and auxiliary complexing species on the distribution of bivalent nickel in liquid-liquid extraction. *J. Chem. Soc. Nig.* **2019**, 44, 661-670.
13. Belskaya, N.P.; Dehaen, W.; Bakulev, V.A. Synthesis and properties of hydrazones bearing amide, thioamide and amidine functions, *Arch. Org. Chem.* **2010**, 1, 275.
14. Ramkisore, U.; Anamika, U.; Dikshit, S.N. Synthesis and spectroscopic studies of bivalent transition metal complexes of Co(II), Ni(II), and Ti(II) with hydrazide-hydrazones. *J. Emerg. Technol. Innov. Res*. **2020**, 5,724-728.
15. Wahbeh, J.; Milkowski, S. The use of hydrazones for biomedical applications. *SLAS Technol.* **2019**, 24, 161-168.
16. Wang, X.; Jaun, Y.; LI, S.; Guoping, Z.; Baoan, S. Design, synthesis, and antibacterial activity of novel Schiff base derivatives of quinazolin-4(3H)-one. *Eur. J. Med. Chem*. **2014**, 77, 65-74.
17. Zaid, S.H.H.; Hai, A.; Nawar, B.R.A. Properties and uses of substituted hydrazones. *J. Pharm. Appl. Chem.* **2018**, 4, 17-21.
18. Radovic, T. *History of In Silico Biology, An Overview.* Novel Global Community Educational Foundation, Australia; **2022**; pp. 1-45.
19. Zhai, P.; Ding, Y.; Wu, X.; Long, J.; Zhong, Y.; Li, Y. The epidemiology, diagnosis and treatment of COVID-19, *Int. J. Antimicrob. Agents* **2020**, 105955.
20. Guo, Y.; Cao, Q.D.; Hong, Z.S.; Tan, Y.Y.; Chen, S.D.; Jin, H.J.; Tan, K.S.; Wang, D.Y.; Yan, Y. The origin, transmission, and clinical therapies on coronavirus disease 2019 (COVID-19) outbreak an update on the status. *Mil. Med. Res*. **2020**, 7, 11.
21. Beigel, J.H.; Tomashek, K.M.; Dodd, L.E.; Mehta, A.K.; Zingman, B.S.; Kalil, A.C.;Hohmann, E.;Chu, H.Y.; Luetkemeyer, A.; Kline, S.; Lopez de Castilla, D.; Finberg, R.W.; Dierberg, K.; Tapson, V.;Hsieh, L.; Patterson, T.F.; Paredes, R.; Sweeney, D.A.; Short, W.R.; Touloumi, G. Remdesivir for the treatment of Covid-19 final report. *New Eng. J. Med.* **2020**, 383, 1813-1826.
22. Lai, A.Y.; Lee, L.; Wang, M.P.; Feng, Y.; Lai, T.T.; Ho, L.M.; Lam, V.S.; Ip, M.S.; Lam, T.H. Mental health impacts of the COVID-19 pandemic on international university students, related stressors, and coping strategies. *Front. Psych.* **2020**, 11, 584240.
23. Devaux, C.A.; Rolain, J.M.; Colson, P.; Raoult, D. New insights on the antiviral effects of chloroquine against coronavirus: what to expect for COVID-19? *Int. J. Antimicrob Agent* **2020**, 55, 105938.
24. Touret, F.; de Lamballerie, X. Of chloroquine and COVID-19. *Antiv. Res*. **2020**, 177, 104762.
25. Al-Bari, M. Targeting endosomal acidification by chloroquine analogs as a promising strategy for the treatment of emerging viral diseases. *Pharmacol. Res. Perspect*. **2017**, 5, e00293.

26. Rebeaud, M.E.; ZoresM, F. SARS-CoV-2 and the use of chloroquine as an Antiviral Treatment. *Front. Med*. **2020**, 7, 184.
27. Al-Tawfiq, J.A.; Al-Homoud, A.H.; Memish. Z.A. Remdesivir as a possible therapeutic option for the COVID-19. *Travel. Med. Infect. Dis.* **2020**, 34, 101615.
28. Morse, J.S.; Lalonde, T.; Xu, S.; Liu. W.R Learning from the Past: Possible Urgent Prevention and Treatment Options for Severe Acute Respiratory Infections Caused by 2019-nCoV. *Eur. J. Chem. Biochem.* **2020**, 21, 730-738.
29. Sheahan, T.P.;Sims, A.C.; Zhou, S.; Graham, R.L.; Pruijssers, A.J.; Agostini, M.L.; Leist, S.R.; Schäfer, A.; Dinnon, L.J.; Stevens, J.D.; Chappell, X..; Lu, T.M.; Hughes, A.S.; George, C.S.; Hill, S.A.; Montgomery, S.A.; Brown, A.J.; Bluemling, G.R.; Natchus, M.G.; Saindane, M.; Baric, R.S. An orally bioavailable broad-spectrum antiviral inhibits SARS-CoV-2 in human airway epithelial cell cultures and multiple coronaviruses in mice. *Sci. transl. Med.* **2020**, 12, eabb5883.
30. He, D.; Zhao, S.; Xu, X.; Lin, Q.; Zhuang, Z.; Cao, P.; Wang, M.H.; Lou, Y.; Xiao, L.; Wu, Y.; Yang, L. Low dispersion in the infectiousness of COVID-19 cases implies difficulty in control. *BMC Pub. Health* **2020**, 20, 1558.
31. Boriskin, Y.S.; Leneva, I.A.; Pécheur, E.I.; Polyak, S.J. Arbidol: A broad-spectrum antiviral compound that blocks viral fusion. *Curr. Med. Chem.* **2008**, 15, 997-1005.
32. Otuokere, I.E.; Chinweuba, A.J. Synthesis, Characterization and fungicidal activity of 3-chloro-4-methyl-N-[(1E)-1-phenylethylidene]aniline ligand and its metal complexes. *J. Chem. Pharm. Res.* **2011**, 6, 905-911.
33. Prushan, M.J. *Lab Manual Advanced Inorganic Chemistry Laboratory*, Department of Chemistry and Biochemistry, La Salle University; **2003**, pp. 3-4.
34. Bouhdada, M.; El Amane, M.; El Hamdani, H.; Khiya, Z. Synthesis, characterization, biological evaluation and molecular docking studies of salicylidene-aniline and their metal mixed ligand complexes with caffeine. *J. Mol. Struct.* **2023,** 1271, 134026-134036.
35. Amadi, C.K.; Atamtürk, U.; Lichtenberg, A.; Raauf, A.; Mathur, S. Undirected C-H bond activation in aluminium hydrido enaminonates. *Mol.* **2023**, 28, 2137-2151.
36. Amadi, C.K.; Karimpour, T.; Jafari, M.; Peng, Z.; Van Gerven, D.; Brune, V.; Hartl, F.; Siaj, M.; Mathur, S. Synthesis and theoretical study of a mixed-ligand indium(III) complex for fabrication of β-In_2S_3 thin films *via* chemical vapor deposition. *Dalton trans.* **2024**, 53, 9874-9886.
37. Ismail, B.A.; Nassar, D.A.; Abd El-Wahab, Z.H.; Ali, O.A.M. Synthesis, characterization, thermal, DFT computational studies and anticancer activity of furfural-type Schiff base complexes. *J. Mol. Struct.* **2021**, 1227, 129393-1293111.
38. Mishra, A.; Sharma, N.; Jain, R. Microwave synthesis, spectral, thermal and antimicrobial studies of some Ni(II) and Cu(II) Schiff base complexes. *Open J. Synth Theory Appl.* **2013**, 2, 56-62.
39. Canpolat, E.; Ağlamiş, A.; Şahal, H.; Kaya, M. Some transition metal complexes of NO type Schiff base: Preparation and characterization, *Cumhuriyet Sci. J.* **2016**, 37, 65-73.
40. Khalf-Alla, P.A.; Hassan, S.S.; Shoukry, M.M. Complex formation equilibria, DFT, docking, antioxidant and antimicrobial studies of iron(III) complexes involving Schiff bases derived from glucosamine or ethanolamine. *Inorg. Chim. Acta* **2019,** 492, 192-197.
41. Rahaman, F.; Gupta, P.; Manjunatha, M.N.; Gautam, P. Benzo [g] indole-based Schiff's base ligand and its transition metal complexes: Synthesis, characterization and anti-microbial activity studies. *Mater. Today Proc.* **2022**, 62, 5598-5604.
42. Otuokere, I.E.; Asogwa, B.C. Sonochemical synthesis and characterization of Fe(II) and Cu(II) nano-sized complexes of sulfamethoxazole. *J. Nig. Soc. Phys. Sci*. **2024**, 6, 1-8.
43. Badal, M.M.R..; Hossain, M.Z.; Maniruzzaman, M. Synthesis, identification and computational studies of novel Schiff bases *N*-(2,6-dibenzylidenecyclohexylidene)-*N′*-(2,4-dinitrophenyl)hydrazine derivatives. *SN Appl. Sci.* **2020**, 2, 1914.